# The Effect of Protein Environment on Photoexcitation Properties of Retinal

Ville R. I. Kaila,*,[†] Robert Send,*,[‡] and Dage Sundholm*,[§]

[†]Laboratory of Chemical Physics, National Institute of Diabetes and Digestive and Kidney Diseases, National Institutes of Health, Bethesda, Maryland 20892, United States

[‡]Institut für Physikalische Chemie, Karlsruher Institut für Technologie, Kaiserstraße 12, 76131 Karlsruhe, Germany

[§]Department of Chemistry, University of Helsinki, P.O. Box 55 (A. I. Virtanens plats 1), FIN-00014 Helsinki, Finland

**S** *Supporting Information*

**ABSTRACT:** Retinal is the photon absorbing chromophore of rhodopsin and other visual pigments, enabling the vertebrate vision process. The effects of the protein environment on the primary photoexcitation process of retinal were studied by time-dependent density functional theory (TDDFT) and the algebraic diagrammatic construction through second order (ADC (2)) combined with our recently introduced reduction of virtual space (RVS) approximation method. The calculations were performed on large full quantum chemical cluster models of the bluecone (BC) and rhodopsin (Rh) pigments with 165−171 atoms. Absorption wavelengths of 441 and 491 nm were obtained at the B3LYP level of theory for the respective models, which agree well with the experimental values of 414 and 498 nm. Electrostatic rather than structural strain effects were shown to dominate the spectral tuning properties of the surrounding protein. The Schiff base retinal and a neighboring Glu-113 residue were found to have comparable proton affinities in the ground state of the BC model, whereas in the excited state, the proton affinity of the Schiff base is 5.9 kcal/mol (0.26 eV) higher. For the ground and excited states of the Rh model, the proton affinity of the Schiff base is 3.2 kcal/mol (0.14 eV) and 7.9 kcal/mol (0.34 eV) higher than for Glu-113, respectively. The protein environment was found to enhance the bond length alternation (BLA) of the retinyl chain and blueshift the first absorption maxima of the protonated Schiff base in the BC and Rh models relative to the chromophore in the gas phase. The protein environment was also found to decrease the intensity of the second excited state, thus improving the quantum yield of the photoexcitation process. Relaxation of the BC model on the excited state potential energy surface led to a vanishing BLA around the isomerization center of the conjugated retinyl chain, rendering the retinal accessible for *cis*−*trans* isomerization. The energy of the relaxed excited state was found to be 30 kcal/mol (1.3 eV) above the minimum ground state energy, and might be related to the transition state of the thermal activation process.
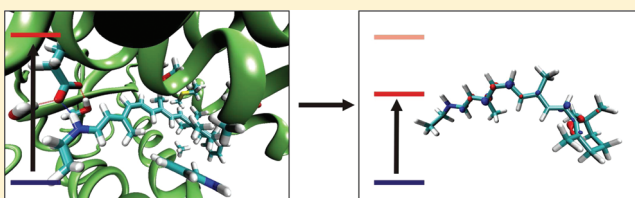
## ■ INTRODUCTION

Rhodopsin (Rh) is a G protein-coupled receptor (GPCR), responsible for light absorption in vertebrate visual pigments.[1,2] The light-absorbing chromophore of Rh is 11-*cis* retinal (Figure 1), which is a conjugated polyene linked to residue Lys-296, forming a Schiff base. Absorption of a photon leads to a *cis*−*trans* isomerization of the retinal chain,[3−7] activating the G protein transducin by conformational changes in the photopigment.[1,2] The activated G protein influences a phosphodiestrase enzyme, which lowers the intracellular cyclic guanosine monophosphate (cGMP) concentration and blocks the influx of cations into the cell. The cell is eventually hyperpolarized as a consequence of the signaling cascade, leading to the vision process.[1,2] In addition to Rh ($\lambda_{max} = 498$ nm), which is the light pigment employed for dim-vision in the rod cells of the retina, color vision is realized in humans by the three cone pigments sensitive for blue ($\lambda_{max} = 414$ nm), green ($\lambda_{max} = 530$ nm), and red ($\lambda_{max} = 560$ nm) light.[8]

Photoisomerization of light pigment-bound retinal is one of the fastest processes in nature, taking place on a femtosecond time scale. After the initial absorption process, 11-*cis* retinal is transformed within 200 fs into photorhodopsin (PHOTO-RH),[7,9,10] followed by 800 fs relaxation to bathorhodopsin (BATHO), which is the first thermodynamically stable all-*trans* retinal state.[4,11,12] The reaction proceeds with the blueshifted intermediate (BS I) within 120 ns,[13] lumirhodopsin (LUMI) within 150 ns, and metarhodopsin I (META I) is formed after 10 $\mu$s.[14,15] In the BATHO to LUMI step, retinal relaxes to a more planar all-*trans* structure.[16] Later states in the photocycle are characterized by a deprotonated Schiff base, many of which have recently been crystallized.[12,17,18] META II, which forms within 1 ms of photoabsorption, is the first intermediate with the ability to initiate signal transduction.[16,19,20] Large-scale protein conformational changes during the LUMI-to-META
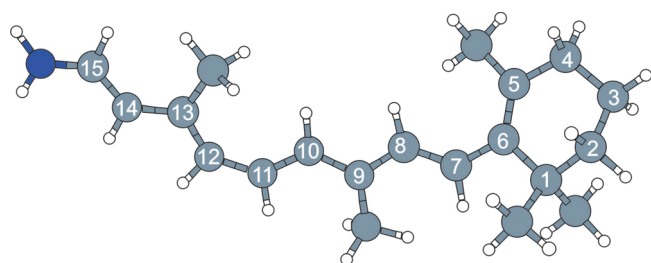
**Figure 1.** The numbering of the carbon atoms of the $\beta$-ionone ring (1−6) and the retinyl chain (7−15) of the light-absorbing 11-*cis* retinal chromophore.

transition have recently been studied by combined biased molecular dynamics simulations and network models.[21]

The protein environment has a profound effect on the absorption spectrum and the photoexcitation process. Photoisomerization is an order of magnitude slower in solution,[22] and the vertical excitation energies of Rh are blueshifted in the protein relative to vacuum and red-shifted relative to methanol,[8,23,24] an effect known as the opsin shift.[25]

Prior to determination of the X-ray structure of Rh, Warshel studied the isomerization process of retinal in a generic protein binding pocket by hybrid semiempirical/classical methods, and predicted that the isomerization takes place in ca. 200 fs.[26] On the basis of these simulations, a "bicycle-pedal" mechanism for the isomerization process was suggested, which involves rotation of two adjacent double bonds.[27] Liu et al.[28,29] proposed a more volume-saving "hula-twist" mechanism involving two neighboring single and double bonds, whereas in the recently proposed "folding table" mechanism of Szymczak et al.,[30,31] three adjacent double bonds participate in the isomerization process. Recent calculations at ab initio correlation levels showed that the retinal skeleton is very flexible on the excited state potential energy surface,[32−34] implying that many of its single and double carbon−carbon bonds may play an active role in the isomerization process.

Color tuning of the absorption spectra of retinals has been suggested to originate from distortions in the chromophore structure,[35,36] electrostatic interactions between the surrounding protein environment and the chromophore,[37−40] as well as from electronic polarization and charge transfer effects leading to changes in the interactions between the positively charged chromophore and negative counterions.[41,42]

Site-directed mutagenesis studies have shown that the absorption maxima of Rh ($\lambda_{max}$ = 498 nm) can be shifted to that of the bluecone (BC) pigment ($\lambda_{max}$ = 414 nm) by mutating several conserved nonpolar residues to more polar residues.[43] Moreover, resonance Raman studies indicate that the skeletal mode vibrations of the chromophore remain nearly unaltered,[8] which is consistent with an electrostatic spectral tuning mechanism. The electrostatic tuning mechanism has also been supported by several computational studies.[44−53]

The chromophore−opsin interaction has previously been studied by quantum mechanical/molecular mechanical (QM/MM) approaches, describing the chromophore at semiempirical,[51,52,54,55] ab initio, (Hartree−Fock,[56] CIS,[57,58] SAC-CI,[49,59] SORCI[55]), density functional theory (DFT, TDDFT[60−63]), and multiconfigurational ab initio (CASSCF,[45,53,64,65] CASPT2,[66,67] MCQDPT2,[63] MRCISD, MR-SORCI+Q,MR-DDCI2+Q[62]) levels with a classical parametrization (AMBER, CHARMM) representing the surrounding protein. The isolated retinal chromophore has also been studied at the DFT[68−72] and quantum Monte Carlo (QMC)[34] levels, as well as using ab initio (CC2,[31,33,69−71,73] CASSCF, CASPT2[34,48,74]) calculations.

We study here the photoexcitation process of retinal in the protein binding pocket of BC and Rh pigments using large full-QM cluster models with 165−171 atoms. Our results are compared with those obtained for the retinal models in gas phase and to previous studies. We employ density functional theory (DFT) and linear-response time-dependent density functional theory (TDDFT) calculations on the retinal chromophore and adjacent parts of the surrounding protein, thus studying the protein-chromophore interactions at a full quantum chemical level of theory. Despite possible shortcomings of TDDFT in describing excited states of anionic chromophores and charge transfer excitations,[72,75−77] recent benchmark studies suggest that the lowest excitation energies of retinal chromophores calculated at the TDDFT/B3LYP level are within a 0.1−0.3 eV agreement with experimental values.[78] The corresponding excitation energies in this benchmarking set obtained at the CC2 level agree slightly better with experiment: typical errors in the CC2 excitation energies are less than 0.15 eV.[78] DFT charge transfer problems are investigated by comparing TDDFT/B3LYP and BHLYP excitation energies and density differences, in addition to values obtained using the algebraic diagrammatic construction through second order (ADC(2)),[79−81] combined with the reduction of virtual space (RVS) approximation method.[82] All studied chromophores are neutral or positively charged, implying that TDDFT calculations on the lowest excited states are not expected to suffer from DFT continuum problems.[32,83] This suggests that TDDFT/B3LYP can be used to study the interaction between retinal and its protein environment at least semiquantitatively at a full quantum mechanical level. Due to the relatively low computational cost and reasonable accuracy of DFT/TDDFT as compared to ab initio approaches, large cluster models of about 200 atoms can be studied, enabling full geometry optimization of the excited state.

## ■ MODELS AND METHODS

Cluster models of the BC and Rh pigments were build based on the homology model and X-rays structure obtained from Brookhaven protein databank (PDB ID: 1KPN[84] and PDB ID: 1HZX,[85] respectively). The protein models comprise 165 and 171 atoms for the respective systems, including Glu-113, Gly-114, Thr-118, Gly-121, −/Glu-122, Ser-186, Pro-189/Ile-189, Leu-207/Met-207, Phe-212, Tyr-265/Trp-265, Ala-269, and Lys-296, in the BC and Rh models, respectively, in addition to the retinal chromophore. The amino acids were modeled in their standard protonation states except Glu-122, which was assumed to be protonated due to the small spectral shift observed in the E122Q mutant[86] and to prevent anionic cluster models.[78] The numbering of amino acid residues refers to the *Bos taurus* protein. A crystallographic water molecule, next to Glu-113, observed in the bovine Rh structure of higher quality (PDB ID: 1U19[87]) was added to both protein models. The amino acid residues were terminated at their $\beta$-carbons, which were fixed in the structure optimizations. Ground-state structures were optimized at the DFT level using the B3LYP functional and the Karlsruhe split-valence quality basis sets augmented with polarization functions (def2-SVP).[88−90] The structures of the Rh and BC models were
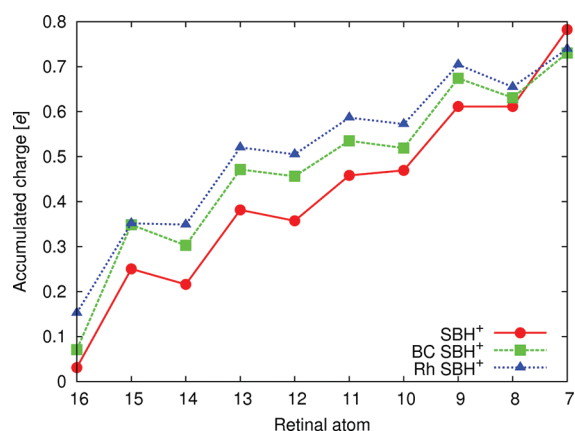
**Figure 2.** The accumulation of the excess charge along the conjugated retinyl chain for the protonated retinals in the BC (BC SBH$^+$) and Rh (Rh SBH$^+$) models as well as for retinal without the protein environment (SBH$^+$).

**Table 1. Effective ESP Charges at the B3LYP/TD-B3LYP Levels Calculated for Different Groups of the Studied BC and Rh Models As Well As for the Isolated Retinals in Gas Phase**[a]

| GS | system | protein | Lys-296 | retinyl | $\beta$-ionone | $Q_{tot}$ | $\mu$ |
|---|---|---|---|---|---|---|---|
| SBH$^+$ | BC | −0.97 | 0.16 | 0.73 | 0.08 | 0.0 | 9.6 |
| SBH$^+$ | Rh | −0.91 | 0.12 | 0.74 | 0.05 | 0.0 | 15.5 |
| SBH$^+$ | vac. | | 0.15 | 0.78 | 0.07 | 1.0 | 19.0 |
| SB | BC | −0.43 | 0.11 | 0.24 | 0.07 | 0.0 | 4.4 |
| SB | Rh | −0.44 | 0.11 | 0.30 | 0.04 | 0.0 | 10.0 |
| SB | vac. | | 0.14 | −0.02 | −0.12 | 0.0 | 3.1 |

| ES | system | protein | Lys-296 | retinyl | $\beta$-ionone | $Q_{tot}$ | $\mu$ |
|---|---|---|---|---|---|---|---|
| SBH$^+$ | BC | −0.94 | 0.14 | 0.55 | 0.26 | 0.0 | 17.3 |
| SBH$^+$ | Rh | −0.78 | 0.10 | 0.53 | 0.16 | 0.0 | 21.9 |
| SBH$^+$ | vac. | | 0.14 | 0.61 | 0.25 | 1.0 | 15.3 |
| SB | BC | −0.43 | 0.09 | 0.11 | 0.23 | 0.0 | 12.9 |
| SB | Rh | −0.43 | 0.08 | 0.18 | 0.17 | 0.0 | 17.4 |
| SB | vac. | | 0.11 | 0.02 | −0.13 | 0.0 | 10.0 |

[a] GS and ES refer to the ESP charges of the ground (GS) and bright excited (ES) states (see Table 2), respectively. The corresponding dipole moments (in Debye) are also given. The Schiff-base nitrogen is included in the charge of the retinal group.

optimized with both protonated (SBH$^+$) and deprotonated Schiff-base retinals (SB), thus with Glu-113 accordingly deprotonated and protonated. The Schiff base N—H distance was constrained to 1.02 Å in the BC SBH$^+$ model, and the Glu-113 O—H distance was constrained to 1.09 Å in the Rh SB model, followed by relaxation of the structures. Single-point energy calculations were also performed on the ground and excited state potential energy surfaces of the isolated chromophore in both protonation states using the chromophore structure taken from the Rh and BC models, followed by optimization without the surrounding protein fragments. The two lowest vertical excitations energies were calculated at the TDDFT level using the B3LYP functional and the Karlsruhe triple-$\zeta$ basis sets augmented with polarization functions (def2-TZVP).[91−96]

In order to identify possible TDDFT charge transfer problems,[75,76] the two lowest vertical excitations energies and corresponding oscillator strengths were also calculated using the BHLYP functional[97] with 50% Hartree−Fock exchange as well as at the ADC(2)[79−81] level combined with the RI approximation[98] and the RVS approach.[82] In the RVS-ADC(2) calculation, virtual orbitals above 20 eV were omitted to reduce the computational cost. According to our benchmarking calculations, this cutoff is expected to lead to an error of 0.3 eV in absolute excitation energies,[82] but to scale similarly for the chromophore in vacuum and embedded in the protein, thus resulting in significantly more accurate protein−chromophore interaction energies.[82]

The molecular structure of the first excited state of the BC model was optimized at the TDDFT/B3LYP/def2-SVP level. Electrostatic potential (ESP) charges for the ground and excited states were also extracted. First-order excited state properties such as excited state charge distributions were calculated analytically. ESP charges for protein residues, Lys-296, the retinyl side chain, and the $\beta$-ionone ring were added together for the ground and excited states. All calculations were performed with TURBOMOLE v. 6.1.[99] VMD was used for analysis and visualization.[100]

### ■ RESULTS

**Ground State.** Optimization of the ground state of the BC model yields a molecular structure with the proton coordinated to Glu-113. When the proton is constrained to reside on the

Schiff base during structure optimization (see Models and Methods), an energetically degenerate structure is obtained, indicating that the residues have comparable proton affinities. Performing the analogous calculations on the Rh model suggest that the Schiff base has a 3.2 kcal/mol higher proton affinity relative to Glu-113. Despite the fact that the calculations suggest that retinal of the BC model is deprotonated in the ground state, the energies are within the expected ground state error marginal of 1−3 kcal/mol of the B3LYP functional.[101,102]

The positive charge of the protonated Schiff base is found to be rather evenly distributed along the retinyl chain in both BC and Rh models (BC SBH$^+$ and Rh SBH$^+$, Figure 2). Relative to gas phase calculations of SBH$^+$, the positive charge is more concentrated to the Schiff base in the protein models, an effect that has been suggested to affect the opsin shift.[8]

The effective electrostatic charges of the protein and the chromophore are given in Table 1. Despite differences in the extent of charge localization (Figure 2), the effective charges of Lys-296, the retinyl side chain, and the $\beta$-ionone ring remain very similar in the two protein models. The retinal is positive with an effective charge of 0.73$e$, whereas the total charge of the surrounding protein residues is close to −1$e$. The protein environment of BC is 0.06$e$ more negative in comparison to the Rh model, which might be the reason for the higher proton affinity of Glu-113 in the former model. When the Schiff base proton is transferred to Glu-113 (BC/Rh SBH$^+$ → BC/Rh SB), the protein obtains an effective charge of −0.43$e$, suggesting that the proton transfer is compensated by a simultaneous transfer of about half an electron from the retinal to surrounding residues.

Despite some differences in the electrostatic effects between the two protein models, the structural properties, measured by the bond length alternation (BLA) of the conjugated retinyl chain, are very similar as shown in Figure 3. The figure shows that the protein environment enhances the BLA of the protonated chromophore, but has a very small effect on the BLA of the deprotonated chromophore (SB). The BLA is also nearly independent regardless of whether the proton resides on the
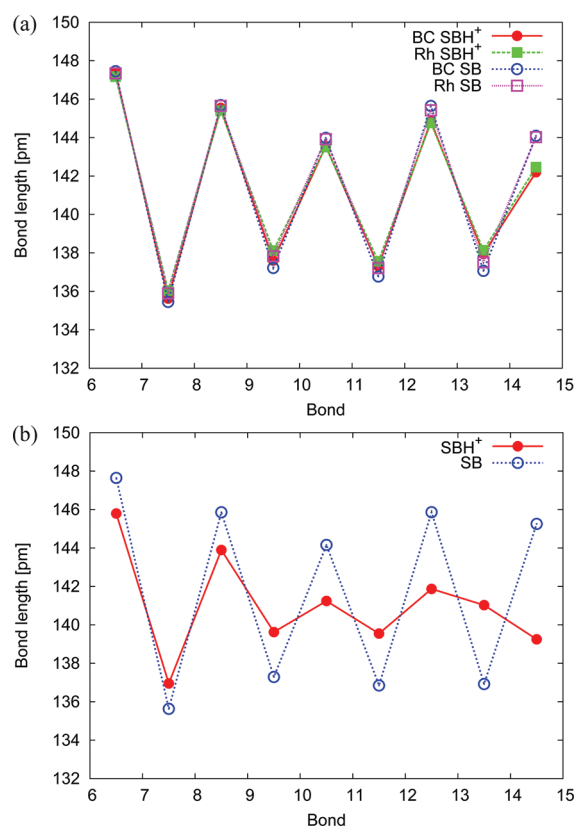
**Figure 3.** (a) The BLA of the ground state of the retinal chromophore of the BC (BC SBH$^+$/BC SB) and Rh models (Rh SBH$^+$/Rh SB). (b) The BLA obtained for retinal in gas phase calculations (SBH$^+$/SB). SBH$^+$/SB denotes the protonation state of retinal-lysine with Glu-113 accordingly deprotonated and protonated, respectively, in the protein models.

**Table 2. Calculated Absorption Wavelengths (in nm) and Corresponding Oscillator Strengths (in Parentheses) for the BC and Rh Models As Well As for the Relaxed and Unrelaxed Structures of the Corresponding Retinals in Gas Phase**[a]

| system | model | es | vacuum | vacuum relax | protein | exp. (protein) |
|--------|-------|----|--------|--------------|---------|----------------|
| BC | SBH$^+$ | 1 | 605 (0.61) | 553 (1.12) | 506 (0.00) | 414 |
|    |         | 2 | 430 (0.74) | 410 (0.65) | 485 (1.07) | |
| BC | SB | 1 | 410 (1.39) | 408 (1.47) | 441 (1.20) | |
|    |    | 2 | 350 (0.00) | 332 (0.00) | 411 (0.00) | |
| Rh | SBH$^+$ | 1 | 568 (0.90) | 553 (1.12) | 491 (1.10) | 498 |
|    |         | 2 | 411 (0.70) | 410 (0.65) | 467 (0.08) | |
| Rh | SB | 1 | 421 (1.49) | 408 (1.47) | 454 (1.28) | |
|    |    | 2 | 367 (0.08) | 332 (0.00) | 413 (0.04) | |

[a] ES 1 and 2 denote the first and second excited state, respectively. Vacuum and vacuum relax refer to the structure of the retinal—lysine moiety obtained from the protein and after structures optimization in vacuum, respectively. The experimental absorption wavelengths for BC and Rh are taken from Nathans.[86]

Schiff base or on Glu-113. This suggests that the different spectral tuning properties of the BC and Rh environments are not determined by geometric properties.

**Vertical Excitations.** Computed absorption wavelengths and corresponding oscillator strengths for BC SBH$^+$, BC SB, Rh SBH$^+$, and Rh SB models are given in Table 2. To distinguish between structural and electronic contributions of the opsin shift, the table also contains absorption wavelengths of the retinal—lysine moiety (SBH$^+$/SB) obtained without the protein environment. These excitation energies are calculated for the chromophore fixed to its structure in the protein (vacuum) and after structure relaxation in vacuum (vacuum relax). To identify possible TDDFT charge transfer problems, the absorption wavelengths and corresponding oscillator strengths were also computed at the TD-BHLYP and RVS20-ADC(2) levels (see Models and Methods), given in Table 3.

**BC Models.** The protein environment blueshifts the absorption wavelength of the first excited state at the TD-B3LYP level of the BC SBH$^+$ model by 47 nm from 553 to 506 nm, whereas the second excited state is red-shifted by 75 nm from 410 to 485 nm (Table 2). The order of these almost degenerate states seem to be interchanged in comparison to the isolated chromophore in gas phase. The two lowest states have large oscillator strengths in the gas phase with the first state slightly brighter. In the BC SBH$^+$ model, the first excited state has a very small oscillator strength and the second state is bright with an oscillator strength

of 1.07. At the TD-BHLYP and RVS20-ADC(2) levels, the order of the two excited states are reversed, with the second excited state shifted higher up in energy, indicating TDDFT charge transfer problems in the TD-B3LYP calculation (Table 3). Reordering of the states is also consistent with dominant orbital contributions shown in Supporting Information (SI) Table 2; at the TD-B3LYP level, the second excited state is characterized by an excitation from the highest occupied molecular orbital (HOMO) to the lowest unoccupied molecular orbital (LUMO), whereas at the TD-BHLYP and RVS20-ADC(2) levels the first excited state has a dominant HOMO → LUMO character. In qualitative agreement with the latter, however, the TD-BHLYP and RVS20-ADC(2) calculations suggest that the protein environment blueshifts the first excited state by 80 and 212 nm, respectively.

For the BC SB model, the protein environment redshifts the absorption wavelength of the two lowest excited states at the TD-B3LYP level. The first is shifted by 33 nm from 408 to 441 nm, and the second by 79 nm from 332 to 411 nm. Proton transfer from the Schiff base to Glu-113 (BC SBH$^+$ → BC SB) blueshifts the first absorption peak of the BC model by 65 nm, which is consistent with experimentally observed shifts of 60 nm due to retinal deprotonation.[41] In ONIOM-type QM/MM calculations with electrostatic embedding,[103] Altun et al.[62] obtained absorption wavelengths of 488 and 402 nm for the first excited state of the protonated and deprotonated retinal Schiff base embedded in the BC pigment. Comparison of the excitation energies obtained in the present full QM calculation with the ONIOM QM/MM energies suggests that QM polarization effects may affect the absorption wavelength by a few tens of nanometers, especially for the second excited state. Similarly to the BC SBH$^+$ model, the TD-BHLYP and RVS20-ADC(2) calculations indicate that the second excited state is affected by TDDFT charge transfer problems (Table 3). The protein environment is predicted to redshift the first excited state by 20 and 28 nm, at the respective levels, which is very close to the protein shift of 33 nm obtained using TD-B3LYP.

The BC pigment has an experimentally determined absorption maximum at 414 nm,[86] which is close to 441 nm obtained for the BC SB model. However, since TD-B3LYP calculations overestimate the excitation energy of the first excited state of the

2252

dx.doi.org/10.1021/jp205918m |*J. Phys. Chem. B* 2012, 116, 2249–2258

**Table 3. Excitation Wavelengths (in nm) Obtained at the TD-B3LYP, TD-BHLYP, and RVS20-ADC(2) Levels**[a]

| system | model | ES | B3LYP | BHLYP | extr. ADC(2)[b] |
|--------|-------|----|-------|-------|-----------------|
| Vacuum | SBH⁺ | 1 | 553 (1.12) | 495 (1.58) | 634 (1.63) |
|        |      | 2 | 410 (0.65) | 342 (0.36) | 399 (0.41) |
| Vacuum | SB   | 1 | 408 (1.47) | 361 (1.92) | 344 (2.26) |
|        |      | 2 | 332 (0.00) | 276 (0.00) | 292 (0.25) |
| BC     | SBH⁺ | 1 | 506 (0.00) | 415 (1.58) | 422 (1.67) |
|        |      | 2 | 485 (1.07) | 293 (0.25) | 300 (0.32) |
| BC     | SB   | 1 | 441 (1.20) | 381 (1.69) | 372 (1.87) |
|        |      | 2 | 411 (0.00) | 274 (0.26) | 306 (0.37) |
| Rh     | SBH⁺ | 1 | 491 (1.10) | 426 (1.64) | 430 (1.77) |
|        |      | 2 | 467 (0.08) | 309 (0.02) | 301 (0.32) |
| Rh     | SB   | 1 | 454 (1.28) | 397 (1.73) | 389 (1.93) |
|        |      | 2 | 413 (0.04) | 282 (0.08) | 313 (0.41) |

[a] Calculated absorption wavelengths (in nm) and corresponding oscillator strengths (in parentheses) for the BC and Rh models as well as for the relaxed structures of the retinals in gas phase (Vacuum). ES 1 and 2 denote the first and second excited state, respectively. [b] Absorption wavelengths are extrapolated from the error introduced by the RVS20 approximation for the isolated SBH⁺ and SB chromospheres in vacuum. Uncorrected excitation wavelengths at the RVS20-ADC(2) levels for the first and second excited states of SBH⁺ and SB are 565, 364, 317, 247 nm.

isolated retinal chromophore by as much as 5−7 kcal/mol (0.3 eV, 80 nm) in worst-case scenarios,[73,78] it remains elusive whether the protonated or deprotonated retinal is the major light absorbing species in BC. Indeed, our recent CC2 calculations on the BC SBH⁺ model predict an absorption wavelength of 424 nm.[82] The excitation energies obtained in the RVS-ADC(2) calculations with a threshold of 20 eV (RVS20), are 0.3 eV smaller than the ones obtained for the SBH⁺ and SB chromophores in vacuum (see footnote in Table 3). The error introduced by the restricted virtual space approximation is practically the same for the chromophore in vacuum as for the chromophore embedded in the protein.[82] This suggests absorption wavelengths of 422 and 372 nm at the ADC(2) level for the BC SBH⁺ and BC SB models, respectively. These values are thus consistent with the recently determined absorption wavelength of 424 nm for the first excited state at the CC2 level.[82]

**Rh Models.** We obtain absorption wavelengths of 491 and 467 nm at the TD-B3LYP level for the two lowest states of the Rh SBH⁺ model. These values agree well with the experimentally determined absorption maximum at 498 nm and with a previously determined value of 505 nm calculated at the TDDFT/QM/MM level.[104] The near-degeneracy of the two lowest excited states of the retinal is supported by absorption measurements in methanol solution.[23] The protein environment blueshifts the first excited state by 62 nm from 553 to 491 nm, which is also in qualitative agreement with experimental observations.[23,43] The second excited state is red-shifted by the protein environment by 57 nm from 410 to 467 nm. Comparison to TD-BHLYP and RVS20-ADC(2) values suggest that the second excited state might suffer from possible charge transfer problems (however, see the Electron Density Differences Induced by Photoexcitation section). The first excited state is similarly to the TD-B3LYP results blueshifted by the protein environment by 69 and 204 nm at the TD-BHLYP and RVS20-ADC(2) levels, respectively.

The two lowest excited states of the Rh SB model absorb at 454 and 413 nm, which are consistent with previous TDDFT/QM/MM estimates of 412−429 nm.[104] Both excited states are red-shifted by the protein environment: the first by 46 nm from 408 to 454 nm, and the second by 81 nm from 332 to 413 nm. Similarly to the Rh SBH⁺ model, TD-BHLYP and RVS20-ADC(2) calculations on the second excited state of Rh SB indicate possible charge transfer problem. The deprotonated chromophore is red-shifted by the protein by 36 and 45 nm at the TD-BHLYP and RVS20-ADC(2) levels, respectively. After correcting for the RVS20 error of 0.3 eV, the absorption wavelengths for the Rh SBH⁺ and Rh SB models at the RVS20-ADC(2) are 440 and 389 nm, respectively.

Similarly to what we observe for the BC SB model at the TD-B3LYP level of theory, the protein environment effectively damps the oscillator strength of the second excited state in the Rh models, which might be of importance for increasing the quantum yield of the photoexcitation process.

**Electrostatic and Strain Effects.** The color tuning properties originating from geometric strain effects can be studied by comparing the spectral shifts due to structure relaxations in vacuum (Table 2). The different contributions obtained at the B3LYP/TD-B3LYP levels, are illustrated in a thermodynamic cycle in Figure 4 (see SI Figure 1 of the SI for the corresponding values obtained using RVS20-ADC(2) calculations).

The relaxed SBH⁺ model has an excitation energy of 51.8 kcal/mol (2.25 eV), which is 4.5 kcal/mol (0.20 eV) higher than the gas phase value of 47.3 kcal/mol (2.05 eV) obtained for the SBH⁺ model frozen to its structure in the BC protein environment (BC SBH⁺, Figure 4). Moreover, the corresponding excitation energy is only 1.5 kcal/mol (0.07 eV) higher than the gas phase value of 50.3 kcal/mol (2.18 eV) obtained for the SBH⁺ model frozen to its structure in the Rh protein environment (Rh SBH⁺). In the gas phase structure relaxations, the ground state relaxes by 6.6 kcal/mol (0.29 eV), whereas the first excited state relaxes by 2.1 kcal/mol (0.09 eV) for the BC SBH⁺ model. The corresponding relaxation effects for the Rh SBH⁺ model are 6.4 kcal/mol (0.28 eV) and 4.9 kcal/mol (0.21 eV), respectively. The increase in excitation energy is thus due to stabilization of the ground state relative to the excited state, suggesting that protein strain effects redshift the absorption maximum.

SBH⁺ embedded in the BC structure (BC SBH⁺ model) has an excitation energy of 59 kcal/mol (2.56 eV), which is red-shifted to 47.3 kcal/mol (2.05 eV) when the protein environment is removed, but the chromophore structure is kept fixed. The electrostatic effect of 11.7 kcal/mol (59−47.3 kcal/mol, 0.51 eV) is thus much larger than the redshift of −4.5 kcal/mol (2.1−6.6 kcal/mol, 0.20 eV) caused by molecular strain effects. A similar analysis for SBH⁺ embedded in the Rh structure (Rh SBH⁺) suggests that electrostatic effects blueshift the first excited state by 8.0 kcal/mol (0.35 eV), which is also larger than the strain effects that redshift the first transition by only −1.5 kcal/mol (4.9−6.4 kcal/mol, 0.07 eV).

SB embedded in the BC structure (BC SB model) has an excitation energy of 64.9 kcal/mol (2.81 eV), which is blueshifted to 69.7 kcal/mol (3.02 eV) when the protein environment is removed, but the chromophore structure is kept fixed. The corresponding values for SB embedded in the Rh structure are 63.0 kcal/mol (2.73 eV) and 67.9 kcal/mol (2.94 eV), suggesting that the electrostatic effects redshift the first excitation energy the by −4.8 kcal/mol and −4.9 kcal/mol (0.21 eV) in BC and Rh, respectively.
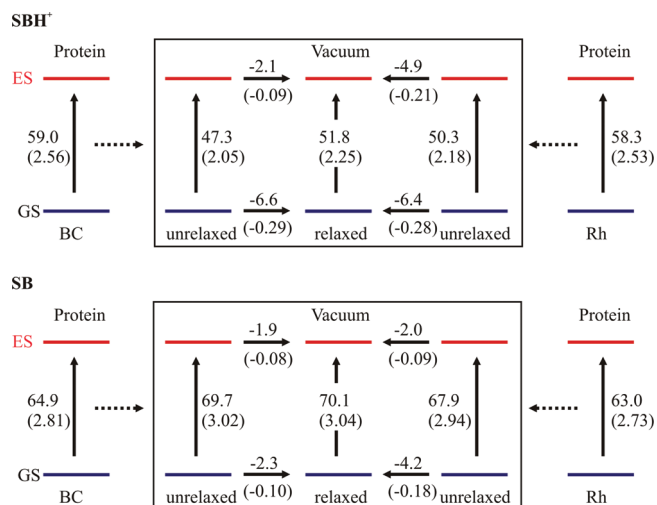
**Figure 4.** Estimated electrostatic and strain effects of the spectral tuning for the BC and Rh models by comparing the relaxation effects of the ground state (GS) and excited state (ES) upon removal of the protein surroundings at the B3LYP/TD-B3LYP levels. The unrelaxed and relaxed energies (in kcal/mol and eV in parentheses) refer to the structure of the retinal-lysine moiety obtained for the protein model before and after structure optimizations in a vacuum, respectively. SBH$^+$/SB denote the protonation state of the retinal-lysine models. Excitation energies refer to the bright states at the TD-B3LYP level (Table 2).

Relaxation of the ground state structure of SB in gas phase gives an excitation energy of 70.1 kcal/mol (3.04 eV). In the relaxation process, the ground and the first excited state are stabilized by 2.3 kcal/mol (0.10 eV) and 1.9 kcal/mol (0.08 eV), respectively. The corresponding ground and excited state relaxation effects in the Rh SB model, are 4.2 kcal/mol (0.18 eV) and 2.0 kcal/mol (0.09 eV), respectively, suggesting that strain effects redshift the absorption by 0.4 kcal/mol (0.02 eV) and 2.2 kcal/mol (0.10 eV) in BC and Rh, respectively.

The electrostatic effects contribute at the TD-B3LYP level to spectral tuning by 5−12 kcal/mol (0.2−0.5 eV), whereas structural strain effects have a smaller effect of 0.4−5 kcal/mol (0.02−0.2 eV), which is also consistent with conclusions reached in earlier studies.[45−53] Electrostatic effects are found to blueshift the first excited state of SBH$^+$, and to red-shifted the first excited state of SB. The second excited state is red-shifted due to electrostatic effects in all protein models. Strain effects also have a redshifting effect on all studied chromophore models. Color tuning properties originating from geometric strain and electrostatic effects were also calculated at the RVS20-ADC(2) level (SI Figure 1). The RVS20-ADC(2) results are qualitatively similar to the TD-B3LYP ones, but predict somewhat stronger electrostatic contributions: the electrostatic effects were found to contribute by 6−20 kcal/mol (0.3−0.9 eV) to spectral tuning, whereas structural strain has a smaller effect of 0.5−3 kcal/mol (0.02−0.14 eV). Moreover, the RVS20-ADC(2) values suggest consistently with the TD-B3LYP calculations that electrostatic effects blueshift the first excited state of SBH$^+$ and redshift the first excited state of SB, whereas strain effects redshift all studied chromophore models.

**Electron Density Differences Induced by Photoexcitation.** Differences in electron densities of the ground and excited states of BC and Rh models and the isolated chromophore in gas phase
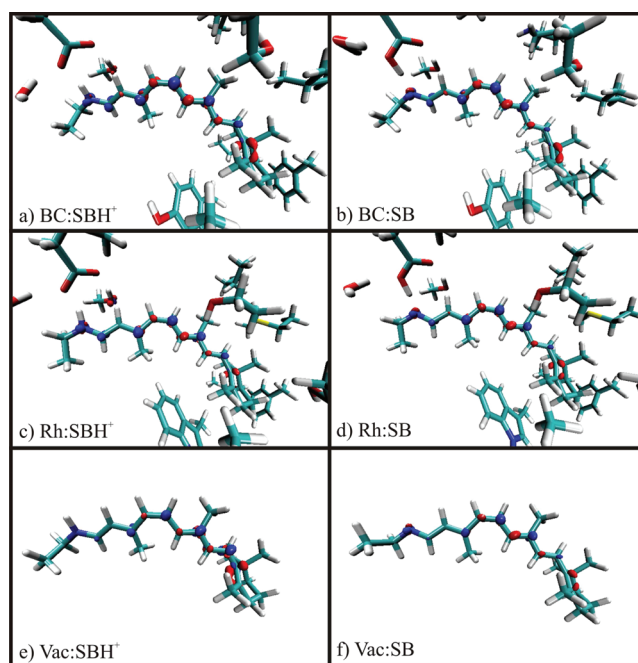


**Figure 5.** Calculated electron density differences at the B3LYP/TD-B3LYP level between the ground and bright excited states (see Table 2) of the BC and Rh models as well as for retinal in gas phase (Vac). (a) The BC model with protonated Schiff base and deprotonated Glu-113, (b) the BC model with deprotonated Schiff base and protonated Glu-113, (c) the Rh model with protonated Schiff base and deprotonated Glu-113, (d) the Rh model with deprotonated Schiff base and protonated Glu-113, (e) the protonated Schiff base in vacuum, and (f) the deprotonated Schiff base in vacuum. Positive (blue) and negative (red) density difference between the excited and ground states are shown as isocontour surfaces using a threshold of ±0.005$e$. Accumulation of positive density difference corresponds to an increase in the negative charge at that region. The figure was prepared with VMD.[100]

are shown in Figure 5. The corresponding effective charges for the ground and excited states are given in Table 1.

The excitation leads to small changes in the electron distribution of the BC SBH$^+$ model. The effective charge of $-1e$ on the protein remains nearly unaffected, whereas 0.18 electrons are transferred from the $\beta$-ionone ring toward the Schiff base, which is also observed for the SBH$^+$ model in vacuum. Photoexcitation of the Rh SBH$^+$ model has in addition to this charge transfer between the $\beta$-ionone ring and the Schiff base, also a small charge transfer of 0.13 electrons from the protein to the retinyl. At the TD-BHLYP level, however, the latter effect is not obtained (see Table 1 of the SI).

The Rh SB and BC SB models show similar differences in the electron density upon excitation. In the ground and excited states, the effective charge of the protein is ca. $-0.4e$, whereas 0.1 electrons are transferred from the $\beta$-ionone ring toward the Schiff base. The effective charges of the isolated chromophore in gas phase calculations show very small changes in the electron distribution of 0.01−0.14 electrons upon photoexcitation.

The blue areas in Figure 5 correspond to accumulations of electron density, and vice versa for red areas. The electron redistribution upon photoexcitation of the protein models (Figure 5a−d) resemble that obtained for the chromophore in gas phase (Figure 5e,f). Negative charge is transferred to the carbon atoms bound to methyl substituents, and positive charge

2254

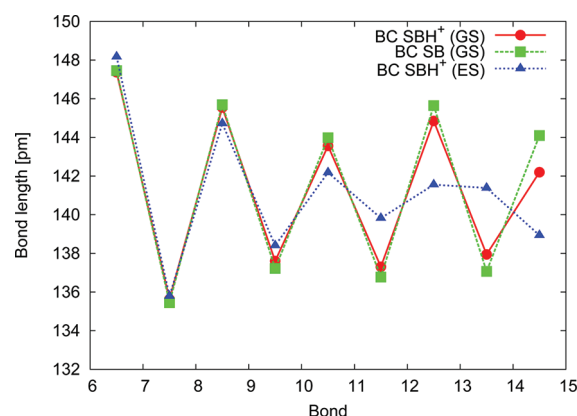dx.doi.org/10.1021/jp205918m | *J. Phys. Chem. B* 2012, 116, 2249−2258

BC



Rh
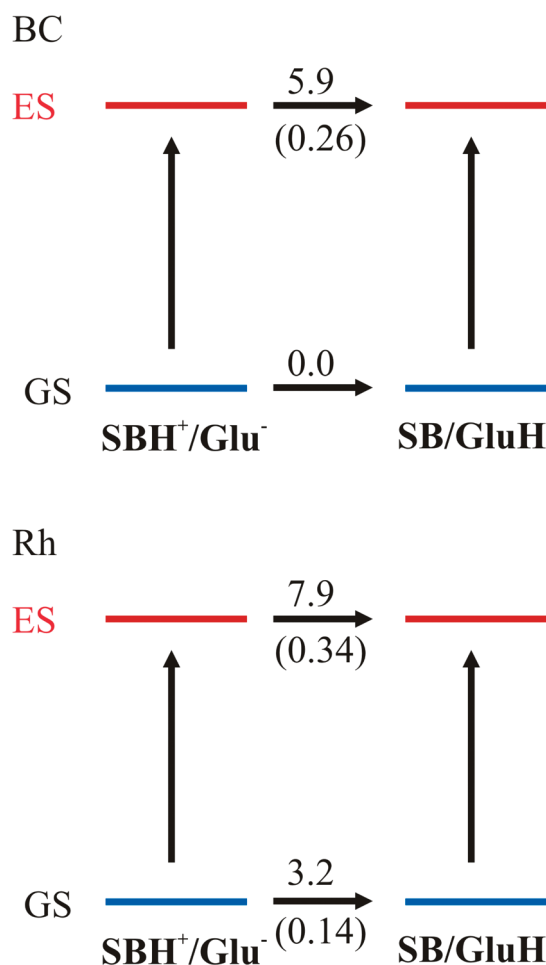


**Figure 6.** Comparison of the relative proton affinities at the B3LYP/TD-B3LYP level in the ground state (GS) and excited state (ES) of the BC and Rh models (in kcal/mol and eV in parentheses). SBH$^+$/SB denote the protonation state of the retinal—lysine moiety, GluH/Glu$^-$ denote the protonation state of Glu-113.



**Figure 7.** The BLA of the retinyl chain of the BC (BC SBH$^+$/BC SB) models in the ground (GS) and excited state (ES) obtained at the B3LYP and TD-B3LYP levels. SBH$^+$/SB denotes the protonation state of the retinal—lysine moiety. The x axis refers to the atom numbering in Figure 1.

accumulates at the $\beta$-ionone ring (Table 1), in agreement with experimental observations.[105,106] This is a likely reason for the strong increase in the dipole moment of 7—9 D in both protein models upon the photoexcitation process (Table 1). Experimentally, retinal photoexcitation is linked to an increase in the dipole moment of 10—15 D.[105,106]

The intramolecular retinal charge transfer shown in Figure 5 leads to an increase in the proton affinity of the Schiff base. In the excited state of the BC model, the proton affinity of the Schiff base is 5.9 kcal/mol (0.26 eV) higher than the proton affinity of Glu-113, whereas the excited Schiff base in Rh has a 7.9 kcal/mol (0.34 eV) higher proton affinity relative to Glu-113 (Figure 6).

The TDDFT charge transfer problems identified in the previous section for the second excited state of the BC SBH$^+$ and BC SB models can be observed as charge transfer from Pro-189 to the $\pi$-electron system of the retinyl chain (SI Figure 2). This effect disappears at the TD-BHLYP level, which corrects for the wrong asymptotic behavior of the TD-B3LYP functional by the increased amount of exact exchange. This is also consistent with the RVS20-ADC(2) calculations, suggesting that the main contribution to the second excited state arises to 90.4% from excitations between occupied and virtual orbitals of the $\pi$-electron

system of the retinyl chain. Comparison of the second excited state at the TD-B3LYP and TD-BHLYP levels for the BC SBH$^+$ and BC SB models suggested a similar charge transfer problem. For the Rh SBH$^+$ and Rh SB models, however, analysis of TD-BHLYP difference densities suggests a similar charge transfer from Trp-265 to the $\pi$-electron system of the retinyl chain, as predicted at the TD-B3LYP level (SI Figure 2). We note that this effect is unlikely to arise from a DFT continuum problem since the energy of the HOMO orbital for all protein models at the TD-B3LYP and TD-BHLYP levels are −5.22 eV to −5.73 eV and −6.09 eV to −6.62 eV, respectively, i.e., well below the DFT ionization energy. RVS20-ADC(2) calculations suggest that the second excited state of Rh SBH$^+$ arises to 64.6% from excitations between occupied and virtual orbitals of the $\pi$-electron system of the retinyl chain, but also to 25.5% from excitations between occupied and virtual orbitals of Trp-265 and the $\pi$-electron system of the retinyl chain (SI Table 2). This charge transfer effect clearly has a different character than the one obtained for the BC model.

**Relaxation of the Excited State.** Optimization of the first excited state of the BC model yields a molecular structure with the proton residing on the Schiff base, in agreement with the increased p$K_a$ of the retinal Schiff base upon photoexcitation. Due to the considerable computational cost of optimizing excited state structures of large molecules at the TDDFT/B3LYP level, the molecular structure was determined only for the first excited state of the BC model. The optimized excited state structure of the BC model has a significant reduction in the BLA of the C—C bonds between $C_{10}$ and $C_{13}$, whereas the $C_{10}$—$C_{11}$—$C_{12}$—$C_{13}$ dihedral angle, which twists during photoisomerization, is decreased by only 2°. The BLA of the ground and excited states of the retinal models are shown in Figure 7. The increased single-bond character of the C—C double bonds at the isomerization center makes the retinyl chain accessible to cis—trans isomerization. However, no other signs of the isomerization process are observed in the excited state structure, implying the existence of a reaction barrier on the excited state potential energy surface, in agreement with experimental observations.[107,108] Moreover, reoptimization of the ground state structure at the BP86/def2-SVP level,[109,110] starting from the optimized excited state structure, yields the initial ground state structure, suggesting that the ground state potential energy surface does not have a significant
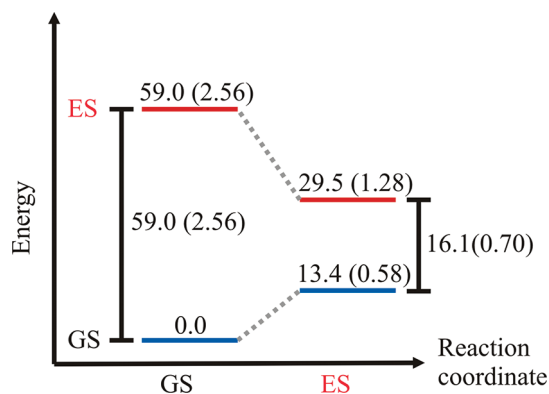
**Figure 8.** Relative energies (in kcal/mol and eV in parentheses) of the ground (GS) and excited state (ES) calculated at the B3LYP/TD-B3LYP levels using the molecular structures of the BC model optimized for the GS and ES, respectively. The reaction coordinate refers to the GS and ES structures. The energy levels on the GS and ES potential energy surface are indicated with black and red lines, respectively.

activation barrier between the relaxed excited and ground state structures.

In the optimization of the excited state, the excitation energy relaxes by 45 kcal/mol (1.95 eV) to 16.1 kcal/mol (0.70 eV), yielding a structure 29.5 kcal/mol (1.28 eV) above the minimum ground state energy (Figure 8). The corresponding increase in the ground state energy of the relaxed excited state structure is 13.4 kcal/mol (0.58 eV).

**Thermal Activation of Rh.** Several molecular mechanisms for the thermal activation of light absorbing pigments have been proposed.[111−114] Barlow et al.[111] suggested that the thermal and light isomerization processes follow different reaction pathways, whereas Ala-Laurila et al.[112] showed by using a subset of contributing vibrational modes and Hinshelwood statistics that the thermal activation barrier is consistent with that of light activation. Lorenz-Fonfria et al.[114] recently suggested using a combination of H/D exchange experiments and IR spectroscopy, that protein fluctuations might be responsible for the thermal activation. The relatively small energy gap between the ground and excited states for the obtained excited state structure could make the excited state potential energy surface accessible by thermal fluctuations. Experimentally, the thermal activation rate corresponds to an activation barrier of 22 kcal/mol (0.95 eV),[2,111,115] a value that has recently been verified by several research groups.[114,116] The optimized structure of the first excited state has a small BLA in the vicinity of the isomerization center, which suggests that many carbon atoms actively participate in the isomerization reaction. Khrenova et al.[63] studied the thermal activation pathway of the retinal isomerization reaction at the DFT/QM/MM level of theory and found a transition state on the ground state potential energy surface between the dark state and BATHO intermediate with an energy of 22 kcal/mol (0.95 eV). The molecular structure of this ground transition state has a large and inverted BLA as compared to the dark state, and thus differs significantly from the present relaxed excited state structure.

## ■ SUMMARY AND CONCLUSIONS

The effects of protein environment on the primary photo-excitation process of retinal have been studied at the DFT and

TDDFT levels using the B3LYP and BHLYP functionals and ADC(2). Amino acid residues in the vicinity of the chromophore of the BC and Rh pigments were included in the studied protein models, which comprised 165−171 atoms and were described at a full quantum chemical level of theory.

For the BC model, the DFT calculations yield comparable ground state p$K_a$ values for the Schiff base retinal and Glu-113, whereas in the Rh model, protonation of the Schiff base is 3.2 kcal/mol (0.14 eV) more favorable than the protonation of Glu-113. In the first excited state, the proton affinity of the Schiff base retinal is 6−8 kcal/mol (0.26−0.35 eV) higher relative to Glu-113. These p$K_a$ shifts can be attributed to electron transfer from the negatively charged protein to the chromophore and to delocalization of the positive charge along the retinyl chain.

The obtained absorption wavelengths for the BC and Rh pigments are 441 and 491 nm for models with deprotonated and protonated Schiff base retinals, respectively, which agree well with the experimental values of 414 and 498 nm, respectively. The corresponding values obtained at the RVS20-ADC(2) level are 372 and 430 nm, after correcting for the systematic error introduced by the RVS approximation. An absorption wavelength of 422 nm is predicted at the RVS20-ADC(2) level for the BC model with a protonated Schiff base retinal. The protein environment was found to blueshift the first absorption maxima of the protonated chromophore by 5−12 kcal/mol (0.2−0.52 eV) due electrostatic interactions, whereas strain effects redshifted the absorption energies by 0.4−5 kcal/mol (0.02−0.22 eV). Electrostatic effects obtained at the RVS20-ADC(2) level were found to be somewhat stronger, 5−20 kcal/mol (0.2−0.9 eV), relative to the TD-B3LYP values, whereas the determined strain effects of 0.5−3.5 kcal/mol (0.02−0.15 eV) were very similar to the TD-B3LYP estimates. TD-B3LYP was found to perform well in describing the first excited state, whereas charge transfer problems for the second excited state of the BC models were identified using TD-BHLYP and RVS20-ADC(2) calculations. A similar charge transfer effect between Trp-265 and the retinyl chain was predicted by TD-B3LYP, TD-BHLYP, and RVS20-ADC(2) calculations for the second excited state of the Rh model. The isolated chromophores in vacuum were not found to be affected by any TDDFT charge transfer problems.

The absorption energies of deprotonated chromophore models were redshifted by both electrostatic and strain effects. The protein environment was also found to enhance the BLA of the conjugated retinyl chain and to decreases the intensity of the second excited state, thus improving the quantum yield of the photoexcitation process.

Structural optimization of the first excited state of the BC model at the TDDFT/B3LYP level yielded a structure lying ca. 30 kcal/mol (1.3 eV) above the ground state energy minimum. The ground state potential energy surface of this structure was found to be 13.4 kcal/mol (0.58 eV) below the excited state potential energy surface. The relaxed excited state energy can be compared to the experimental thermal activation energy of 22 kcal/mol (0.95 eV).[2,111,115] The retinyl chain of the first excited state of the BC pigment has a vanishing BLA at the isomerization center of the conjugated retinyl chain, which most likely renders the retinal accessible for *cis*−*trans* isomerization. The excited state structure does not show any significant torsional changes of the retinyl $C_{11}$−$C_{12}$ double bond, which would indicate a *cis*−*trans* isomerization. Reoptimization of the ground state, starting from the excited state structure led back to the initially optimized ground state structure, implying that the minima of

the ground and excited state potential energy surfaces are not separated by any significant energy barrier.

## ■ ASSOCIATED CONTENT

**ⓢ Supporting Information.** Two figures and two tables with electrostatic/strain effects, electron density differences, effective ESP charges, and dominant orbital contributions. This information is available free of charge via the Internet at http://pubs.acs.org/.

## ■ AUTHOR INFORMATION

**Corresponding Author**
*E-mail: ville.kaila@nih.gov (V.R.I.K.); robert.send@kit.edu (R.S.); sundholm@chem.helsinki.fi (D.S.).

## ■ ACKNOWLEDGMENT

## ■ REFERENCES

(1) Palczewski, K. *Annu. Rev. Biochem.* **2006**, *75*, 743–767.

(2) Burns, M. E.; Baylor, D. A. *Annu. Rev. Neurosci.* **2001**, *24*, 779–805.

(3) Wald, G. *Science* **1968**, *162*, 230–239.

(4) Kukura, P.; McCamant, D. W.; Yoon, S.; Wandschneider, D. B.; Mathies, R. A. *Science* **2005**, *310*, 1006–1009.

(5) Kandori, H.; Furutani, Y.; Nishimura, S.; Shichida, Y.; Chosrowjan, H.; Shibata, Y.; Mataga, N. *Chem. Phys. Lett.* **2001**, *334*, 271–276.

(6) Becker, R. S.; Freedman, K. *J. Am. Chem. Soc.* **1985**, *107*, 1477–1485.

(7) Kakitani, T.; Akiyama, R.; Hatano, Y.; Imamoto, Y.; Shichida, Y.; Verdegem, P.; Lugtenburg, J. *J. Phys. Chem. B* **1998**, *102*, 1334–1339.

(8) Kochendoerfera, G. G.; Lin, S. W.; Sakmar, T. P.; Mathies, R. A. *Trends Biochem. Sci.* **1999**, *24*, 300–305.

(9) Shichida, Y. *Photobiochem. Photobiophys.* **1986**, *13*, 287–307.

(10) Schoenlein, R. W.; Peteanu, L. A.; Mathies, R. A.; Shank, C. V. *Science* **1991**, *254*, 412–415.

(11) Yoshizawa, T.; Kito, Y. *Nature* **1958**, *182*, 1604–1605.

(12) Nakamichi, H.; Okada, T. *Angew. Chem., Int. Ed.* **2006**, *45*, 4270–4273.

(13) Hug, S. J.; Lewis, J. W.; Einterz, C. M.; Thorgeirsson, T. E.; Kliger, D. S. *Biochemistry* **1990**, *29*, 1475–1485.

(14) Okada, T.; Ernst, O. P.; Palczewski, K.; Hoffmann, K. P. *Trends Biochem. Sci.* **2001**, *26*, 318–324.

(15) Jäger, S.; Lewis, J. W.; Zvyaga, T. A.; Szundi, I.; Sakmar, T. P.; Kliger, D. S. *Proc. Natl. Acad. Sci. U.S.A.* **1997**, *94*, 8557–8562.

(16) Pan, D. H.; Mathies, R. A. *Biochemistry* **2001**, *40*, 7929–7936.

(17) Jäger, F.; Fahmy, K.; Sakmar, T. P.; Siebert, F. *Biochemistry* **1994**, *33*, 10878–10882.

(18) Nakamichi, H.; Okada, T. *Proc. Natl. Acad. Sci. U.S.A.* **2006**, *103*, 12729–12734.

(19) Kliger, D. S.; Lewis, J. W. *Isr. J. Chem.* **1995**, *35*, 289–307.

(20) Arnis, S.; Hofmann, K. P. *Proc. Natl. Acad. Sci. U.S.A.* **1993**, *90*, 7849–7853.

(21) Tikhonova, I. G.; Best, R. B.; Engel, S.; Gershengorn, M. C.; Hummer, G.; Costanzi, S. *J. Am. Chem. Soc.* **2008**, *130*, 10141–10149.

(22) Logunov, S. L.; Song, L.; El-Sayed, M. A. *J. Phys. Chem.* **1996**, *100*, 18586–18591.

(23) Nielsen, I. B.; Lammich, L.; Andersen, L. H. *Phys. Rev. Lett.* **2006**, *96*, 018304.

(24) Nielsen, M. B. *Chem. Soc. Rev.* **2009**, *38*, 913–924.

(25) Honig, B.; Dinur, U.; Nakanishi, K.; Balogh-Nair, V.; Gavinowicz, M. A.; Arnaboldi, M.; Motto, M. G. *J. Am. Chem. Soc.* **1979**, *101*, 7084–7086.

(26) Warshel, A. *Nature* **1976**, *260*, 679–683.

(27) Schapiro, I.; Weingart, O.; Buss, V. *J. Am. Chem. Soc.* **2009**, *131*, 16–17.

(28) Liu, R. S. H.; Asato, A. E. *Proc. Natl. Acad. Sci. U.S.A.* **1985**, *82*, 259–263.

(29) Liu, R. S. H.; Hammond, G. S. *Chem.—Eur. J.* **2001**, *7*, 4536–4544.

(30) Szymczak, J. J.; Barbatti, M.; Lischka, H. *J. Chem. Theory Comput.* **2008**, *4*, 1189–1199.

(31) Szymczak, J. J.; Barbatti, M.; Lischka, H. *J. Phys. Chem. A* **2009**, *113*, 11907–11918.

(32) Lehtonen, O.; Sundholm, D.; Send, R.; Johansson, M. P. *J. Chem. Phys.* **2009**, *131*, 024301.

(33) Send, R.; Sundholm, D.; Johansson, M. P.; Pawłowski, F. *J. Chem. Theory Comput.* **2009**, *5*, 2401–2414.

(34) Valsson, O.; Filippi, C. *J. Chem. Theory Comput.* **2010**, *6*, 1275–1292.

(35) Blatz, P. E.; Liebman, P. *Exp. Eye Res.* **1973**, *17*, 573–580.

(36) Kakitani, H.; Kakitani, T.; Rodman, H.; Honig, B. *Photochem. Photobiol.* **1985**, *41*, 471–479.

(37) Kropf, A.; Hubbard, R. *Ann. N.Y. Acad. Sci.* **1958**, *74*, 266–280.

(38) Honig, B.; Greenberg, A. D.; Dinur, U.; Ebrey, T. G. *Biochemistry* **1976**, *15*, 4593–4599.

(39) Neitz, M.; Neitz, J.; Jacobs, G. H. *Science* **1991**, *252*, 971–974.

(40) Beppu, Y.; Kakitani, T. *Photochem. Photobiol.* **1994**, *59*, 660–669.

(41) Morton, R. A.; Pitt, G. A. J. *Biochem. J.* **1955**, *59*, 128–134.

(42) Baasov, T.; Friedman, N.; Sheves, M. *Biochemistry* **1987**, *26*, 3210–3217.

(43) Lin, S. W.; Kochendoerfer, G. G.; Carroll, H. S.; Wang, D.; Mathies, R. A.; Sakmar, T. P. *J. Biol. Chem.* **1998**, *273*, 24583–24591.

(44) Fujimoto, K.; Hayashi, S.; Hasegawa, J.; Nakatsuji, H. *J. Chem. Theory Comput.* **2007**, *3*, 605–618.

(45) Hayashi, S.; Tajkhorshid, E.; Pebay-Peyroula, E.; Royant, A.; Landau, E. M.; Navarro, J.; Schulten, K. *J. Phys. Chem. B* **2001**, *105*, 10124–10131.

(46) Schreiber, M.; Buss, V.; Sugihara, M. *J. Chem. Phys.* **2003**, *119*, 12045–12048.

(47) Wanko, M.; Hoffmann, M.; Strodel, P.; Koslowski, A.; Thiel, W.; Neese, F.; Frauenheim, T.; Elstner, M. *J. Phys. Chem. B* **2005**, *109*, 3606–3615.

(48) Andruniów, T.; Ferré, N.; Olivucci, M. *Proc. Natl. Acad. Sci. U.S.A.* **2004**, *101*, 17908–17913.

(49) Fujimoto, K.; Hasegawa, J. Y.; Hayashi, S.; Kato, S.; Nakatsuji, H. *Chem. Phys. Lett.* **2005**, *414*, 239–242.

(50) Sakurai, M.; Sakata, K.; Saito, S.; Nakajima, S.; Inoue, Y. *J. Am. Chem. Soc.* **2003**, *125*, 3108–3112.

(51) Warshel, A.; Chu, Z. T. *J. Phys. Chem. B* **2001**, *105*, 9857–9871.

(52) Houjou, H.; Inoue, Y.; Sakurai, M. *J. Phys. Chem. B* **2001**, *105*, 867–879.

(53) Hayashi, S.; Ohmine, I. *J. Phys. Chem. B* **2000**, *104*, 10678–10691.

(54) Matsuura, A.; Sato, H.; Houjou, H.; Saito, S.; Hayashi, T.; Sakurai, M. *J. Comput. Chem.* **2006**, *27*, 1623–1630.

(55) Hoffmann, M.; Wanko, M.; Strodel, P.; König, P. H.; Frauenheim, T.; Schulten, K.; Thiel, W.; Tajkhorshid, E.; Elstner, M. *J. Am. Chem. Soc.* **2006**, *128*, 10808–10818.

(56) Yamada, A.; Kakitani, T.; Yamamoto, S.; Yamato, T. *Chem. Phys. Lett.* **2002**, *366*, 670–675.

(57) Rajamani, R.; Gao, J. L. *J. Comput. Chem.* **2002**, *23*, 96–105.

(58) Trabanino, R. J.; Vaidehi, N.; Goddard, W. A. *J. Phys. Chem. B* **2006**, *110*, 17230–17239.

(59) Fujimoto, K.; Hasegawa, J.; Nakatsuji, H. *Chem. Phys. Lett.* **2008**, *462*, 318–320.

(60) Gascón, J. A.; Sproviero, E. M.; Batista, V. S. *Acc. Chem. Res.* **2006**, *39*, 184–193.

(61) Röhrig, U. F.; Sebastiani, D. *J. Phys. Chem. B* **2008**, *112*, 1267–1274.

(62) Altun, A.; Yokoyama, S.; Morokuma, K. *J. Phys. Chem. A* **2009**, *113*, 11685–11692.

(63) Khrenova, M. G.; Bochenkova, A. V.; Nemukhin, A. V. *Proteins* **2010**, *78*, 614–622.

(64) Hayashi, S.; Tajkhorshid, E.; Schulten, K. *Biophys. J.* **2002**, *83*, 1281–1297.

(65) Hayashi, S.; Tajkhorshid, E.; Schulten, K. *Biophys. J.* **2009**, *96*, 403–416.

(66) Ferré, N.; Olivucci, M. *J. Am. Chem. Soc.* **2003**, *125*, 6868–6869.

(67) Coto, P. B.; Sinicropi, A.; De Vico, L.; Ferre, N.; Olivucci, M. *Mol. Phys.* **2006**, *104*, 983–991.

(68) Blomgren, F.; Larsson, S. *J. Phys. Chem. B* **2005**, *109*, 9104–9110.

(69) Send, R.; Sundholm, D. *J. Phys. Chem. A* **2007**, *111*, 27–33.

(70) Send, R.; Sundholm, D. *J. Phys. Chem. A* **2007**, *111*, 8766–8773.

(71) Send, R.; Sundholm, D. *J. Mol. Model.* **2008**, *14*, 717–726.

(72) Rostov, I. V.; Amos, R. D.; Kobayashi, R.; Scalmani, G.; Frisch, M. J. *J. Phys. Chem. B* **2010**, *114*, 5547–5555.

(73) Send, R.; Sundholm, D. *Phys. Chem. Chem. Phys.* **2007**, *9*, 2862–2867.

(74) Sekharan, S.; Weingart, O.; Buss, V. *Biophys. J.* **2006**, *91*, L07–L09.

(75) Wanko, M.; Garavelli, M.; Bernardi, F.; Niehaus, T. A.; Frauenheim, T.; Elstner, M. *J. Chem. Phys.* **2004**, *120*, 1674–1692.

(76) Dreuw, A.; Head-Gordon, M. *Chem. Rev.* **2005**, *105*, 4009–4037.

(77) Yanai, T.; Tew, D. P.; Handy, N. C. *Chem. Phys. Lett.* **2004**, *393*, 51–57.

(78) Send, R.; Kaila, V. R. I.; Sundholm, D. *J. Chem. Theory Comput.* **2011**, *7*, 2473–2484.

(79) Schirmer, J. *Phys. Rev. A* **1982**, *26*, 2395–2416.

(80) Trofimov, A. B.; Schirmer, J. *J. Phys. Chem. B* **1995**, *28*, 2299–2324.

(81) Hättig, C. *Adv. Quantum Chem.* **2005**, *50*, 37–60.

(82) Send, R.; Kaila, V. R. I.; Sundholm, D. *J. Chem. Phys.* **2011**, *134*, 214114.

(83) Casida, M. E.; Jamorski, C.; Casida, K. C.; Salahub, D. R. *J. Chem. Phys.* **1998**, *108*, 4439–4449.

(84) Stenkamp, R. E.; Filipek, S.; Driessen, C. A. G. G.; Teller, D. C.; Palczewski, K. *Biochim. Biophys. Acta* **2002**, *1565*, 168–182.

(85) Teller, D. C.; Okada, T.; Behnke, C. A.; Palczewski, K.; Stenkamp, R. E. *Biochemistry* **2001**, *40*, 7761–7772.

(86) Nathans, J. *Biochemistry* **1990**, *29*, 937–942.

(87) Okada, T.; Sugihara, M.; Bondar, A. N.; Elstner, M.; Entel, P.; Buss, V. *J. Mol. Biol.* **2004**, *342*, 571–583.

(88) Lee, C.; Yang, W.; Parr, R. G. *Phys. Rev. B* **1988**, *37*, 785–789.

(89) Becke, A. D. *J. Chem. Phys.* **1993**, *98*, 5648–5652.

(90) Schäfer, A.; Horn, H.; Ahlrichs, R. *J. Chem. Phys.* **1992**, *97*, 2571–2577.

(91) Bauernschmitt, R.; Ahlrichs, R. *Chem. Phys. Lett.* **1996**, *256*, 454–464.

(92) Furche, F.; Ahlrichs, R. *J. Chem. Phys.* **2002**, *117*, 7433–7447.

(93) Furche, F.; Ahlrichs, R. *J. Chem. Phys.* **2004**, *121*, 12772–12773.

(94) Schäfer, A.; Huber, C.; Ahlrichs, R. *J. Chem. Phys.* **1994**, *100*, 5829–5835.

(95) Weigend, F.; Häser, M.; Patzelt, H.; Ahlrichs, R. *Chem. Phys. Lett.* **1998**, *294*, 143–152.

(96) Weigend, F.; Ahlrichs, R. *Phys. Chem. Chem. Phys.* **2005**, *7*, 3297–3305.

(97) Becke, A. D. *J. Chem. Phys.* **1993**, *98*, 1372–1377.

(98) Hättig, C.; Weigend, F. *J. Chem. Phys.* **2000**, *113*, 5154–5161.

(99) Ahlrichs, R.; Bär, M.; Häser, M.; Horn, H.; Kölmel, C. *Chem. Phys. Lett.* **1989**, *162*, 165–169current version: see http://www.turbomole.com.

(100) Humphrey, W.; Dalke, A.; Schulten, K. *J. Mol. Graphics* **1996**, *14*, 33–38.

(101) Curtiss, L. A.; Raghavachari, K.; Trucks, G. W.; Pople, J. A. *J. Chem. Phys.* **1991**, *94*, 7221–7230.

(102) Curtiss, L. A.; Raghavachari, K.; Redfern, R. C.; Pople, J. A. *J. Chem. Phys.* **2000**, *112*, 7374–7383.

(103) Vreven, T.; Byun, K. S.; Komaromi, I.; Dapprich, S.; Montgomery, J. A.; Morokuma, K.; Frisch, M. J. *J. Chem. Theory Comput.* **2006**, *2*, 815–826.

(104) Altun, A.; Yokoyama, S.; Morokuma, K. *J. Phys. Chem. B* **2008**, *112*, 16883–16890.

(105) Mathies, R. A.; Stryer, L. *Proc. Natl. Acad. Sci. U.S.A.* **1976**, *73*, 2169–2173.

(106) Birge, R. R.; Murray, L. P.; Pierce, B. M.; Akita, H.; Balogh-Nair, V.; Findsen, L.; Nakanishi, K. *Proc. Natl. Acad. Sci. U.S.A.* **1985**, *82*, 4117–4121.

(107) Yoshizawa, T.; Shichida, Y.; Matuoka, S. *Vision Res.* **1984**, *24*, 1455–1463.

(108) Gai, F.; Hasson, K. C.; McDonald, J. C.; Anfinrud, P. A. *Science* **1998**, *279*, 1886–1891.

(109) Becke, A. D. *Phys. Rev. A* **1988**, *38*, 3098–3100.

(110) Perdew, J. P. *Phys. Rev. B* **1986**, *33*, 8822–8824.

(111) Barlow, R. B.; Birge, R. R.; Kaplan, E.; Tallent, J. R. *Nature* **1993**, *366*, 64–66.

(112) Ala-Laurila, P.; Donner, K.; Koskelainen, A. *Biophys. J.* **2004**, *86*, 3653–3662.

(113) Ala-Laurila, P.; Donner, K.; Crouch, R. K.; Cornwall, M. C. *J. Physiol.* **2007**, *585*, 57–74.

(114) Lórenz-Fonfría, V. A.; Furutani, Y.; Ota, T.; Ido, K.; Kandori, H. *J. Am. Chem. Soc.* **2010**, *132*, 5693–5703.

(115) Baylor, D. A.; Matthews, G.; Yau, K. W. *J. Physiol.* **1980**, *309*, 591–621.

(116) Silva López, C.; Álvarez, R.; Domínguez, M.; Nieto Faza, O.; de Lera, A. R. *J. Org. Chem.* **2009**, *74*, 1007–1013.